One-Pot Solvothermal Synthesis of ZnSe·xN$_2$H$_4$/GS and ZnSe/N-GS and Enhanced Visible-Light Photocatalysis

Bitao Liu,[†,‡,*] Liangliang Tian,*,[†] and Yuhua Wang[‡]

[†]Chongqing Key Laboratory of Micro/Nano Materials Engineering and Technology, Chongqing University of Arts and Science, Chongqing 402160, PR China

[‡]Department of Materials Science, School of Physical Science and Technology, Lanzhou University, Lanzhou, 730000, PR China

Ⓢ *Supporting Information*

ABSTRACT: Doped-graphene has attracted considerable attention in many fields because doping element can alter the electrical properties of graphene. In this paper, we synthesized ZnSe·xN$_2$H$_4$/graphene (ZnSe·xN$_2$H$_4$/GS) and ZnSe/nitrogen-doped graphene (ZnSe/N-GS) nanocomposites with p-n junctions via one-pot solvothermal process. The structure, morphologies and catalytic performance of the ZnSe·xN$_2$H$_4$/GS and ZnSe/N-GS are characterized by X-ray diffraction pattern (XRD), field emission scanning electron microscopy (SEM), transmission electron microscopy (TEM), Raman spectroscopy (RS), X-ray photoelectron spectroscopy (XPS), and cathodoluminescence spectrum (CL), respectively.

Our experiments show that the as-prepared nanocomposites ZnSe·xN$_2$H$_4$/GS and ZnSe/N-GS exhibit remarkably enhanced photocatalytic activities for methylene blue (MB) dye under visible light irradiation. Even importantly, ZnSe/N-GS would make this degradation process more effective. Overall, this facile and catalyst-free synthesize method in this work could provide new insights into the fabrication of other composites based on doped graphene with high performance photocatalysts, which show their potential applications in producing of hydrogen through water splitting, environmental protection issues.

KEYWORDS: *ZnSe, graphene, photocatalyst, nanocomposites*
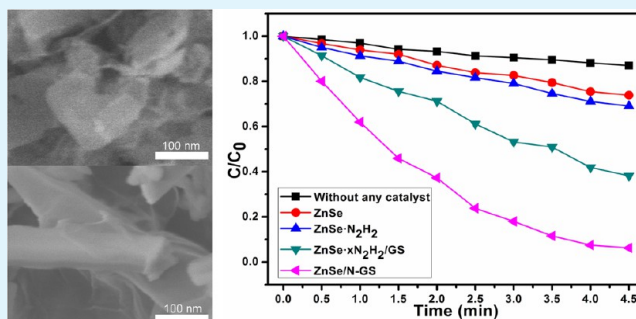
■ INTRODUCTION

Graphene sheet (GS), a two dimensional monolayer form of hexagonally arrayed sp^2-bonded carbon atoms, is a rapidly rising star on the horizon of materials science and condensed matter physics because it exhibits excellent physical and chemical properties.[1,2] It has high thermal conductivities (5300 Wm^{-1} K^{-1}),[3] excellent intrinsic mobility limit (2×10^5 cm^2 V^{-1} s^{-1}),[4] great mechanical strength,[5] huge specific surface area (SSA ≈ 2630 m^2 g^{-1})[6,7] and good transparency.[8] Graphene can be obtained through different methods, one is the "top−down" approach involving the chemical exfoliation of graphite[9] or the longitudinal "unzipping" of carbon nanotubes (CNTs),[10,11] the other is "bottom−up" epitaxial growth method via chemical vapor deposition (CVD)[12,13] or organic synthesis.[14] Doped-graphene will be the key to its future applications because doping can alter electrical and chemical properties for graphene.[15,16] Nitrogen-doped graphene,[17] boron-doped graphene,[18] Li-doped graphene,[19] and aromatic molecules-doped graphene[20] have been synthesized. Especially, nitrogen-doped graphene have widespread applications in many fields, including catalysts, ultracapacitors and the area of clean energy.[17,21] But it is still a challenge to prepare nitrogen-doped graphene and its composites by a facile method.[17]

Semiconductor nanostructures have attracted intensive interest because of their fundamental importance, as well as their enormous potential in optoelectronic, magnetic, and catalytic applications.[22,23] As one of the Zn-based II−VI semiconductors, zinc selenide (ZnSe), a direct band gap semiconductor with band gap energy of 2.7 eV, is regarded as a good candidate for short-wavelength lasers, blue laser diodes, light-emitting diodes, and tunable mid-IR laser sources.[24] Recently, nanostructure ZnSe such as zero-dimensional ZnSe nanoparticles, one dimensional ZnSe nanowires, and two-dimensional ZnSe thin films have been extensively investigated.[25,26] Yu et al. have prepared uniform and well-defined ZnSe-(diethylenetriamine)0.5([ZnSe](DETA)0.5) nanobelts by hydrazine-hydrate assisted solvothermal reactions in a ternary solution. This nanobelt is an inorganic−organic hybrid material, which consists of ZnSe slabs sandwiched by coordinated diethylenetriamine layers.[27]

On the basis of the unique properties of graphene, considerable efforts have been made to incorporate graphene sheets in a composite material. To date, a great number of inorganic nanostructures, such as Cu, Au, Ag, TiO$_2$, ZnO, SnO$_2$, CdS, and CdSe, have been composited with graphene for applications, including batteries, supercapacitors, fuel cells,

photovoltaic devices, photocatalysis, sensing platforms, and Raman enhancement.[28−35] Since graphene nanocomposites can exhibit enhanced performance, it has become a priority for researchers to prepare these nanocomposites.[36] However, only Chen et al.[37] reported the synthesis of nitrogen-doped graphene/ZnSe nanorod nanocomposites via a two step process. To the best of our knowledge, little work has been done on graphene/doped graphene-based ZnSe nanobelt.

Herein, in this work, graphene/doped graphene-based ZnSe nanobelt was prepared by a facile one-pot solvothermal process. And its synthesis process and photocatalytic properties were investigated in detail.

■ EXPERIMENTAL SECTION

Preparation of GO Dispersion. Graphene oxide (GO) was prepared by oxidation of natural graphite powder by a modified Hummers method.[38] Details are presented in Supporting Information. Synthesis of nitrogen-doped ZnSe·xN_2H_4/GS and ZnSe/N-GS nanocomposites

All chemicals used in this experiment were of analytical grade and were used as received without further purification. The preparation of nitrogen-doped graphene/ZnSe nanocomposites were performed by a one-pot approach. In a typical procedure, 0.0439 g $Zn(AC)_2$·$2H_2O$ (0.2 mmol) was dissolved in 6 mL of DI water to form a transparent solution under magnetic stirring. Na_2SeO_3·$5H_2O$ (0.0526 g), 3 mL of GO dispersion (9.3 g L^{-1}), and 12 mL of N_2H_4·H_2O (80%) were sequentially added. Then the mixed solution was sonicated for 1.5 h and transferred to a Teflon-lined autoclave of 30 mL capacity. The autoclave was sealed and maintained at 180 °C for 12 h, and then cooled naturally to room temperature. After the reaction was completed, the solution was filtered, washed sequentially with DI water and absolute ethanol, and dried by freeze drying. And a contrast sample was synthesized with adding 0.1489 g of EDTA−2Na (0.4 mmol) in the same reaction conditions.

Characterization and Measurements. The crystal structure and phase of the synthesized products were characterized by powder X-ray diffraction (XRD, Rigaku D/MAX-2400 X-ray diffractometer with Ni-filtered Cu K$_\alpha$ radiation). X-ray photoelectron spectroscopy (XPS, PHI-5702, Physical Electronics) was performed using a monochromated Al Kα irradiation. Raman spectroscopy (Renishaw inVia Raman microscope with 633 nm line of an Ar ion laser as an excitation source) was employed to characterize the microstructure of the samples. The morphology and microstructures were observed by a field emission scanning electron microscope (FESEM, Hitachi, S-4800), transmission electron microscopy (TEM) and high-resolution transmission electron microscopy (HRTEM, FEI Tecnai F30, operated at 300 kV). Peak deconvolution and quantification of elements were accomplished using Origin 8.0. Low-voltage CL spectra were obtained using a modified Mp-Micro-S instrument. Fluorescence lifetimes were measured on a Perkin-Elmer LS 50B spectrofluorimeter by the time-correlated single-photon counting method.

The liquid-phase photodegradation of dyes (methylene blue) was carried out in a quartz tube under the irradiation of UV light. And the concentration of MB solution was analyzed by measuring the light absorption of the clear solution at 664 nm, respectively.

■ RESULTS AND DISCUSSION

Figure 1 shows the typical XRD patterns of the samples obtained by one-pot solvothermal process in comparison to the patterns of GO and RGO. Obviously, there is no XRD peak at 10.7° and a broad peak at around 23.3° with a d-spacing of 0.4 nm appears, implying that the oxygen-containing functional groups of GO can be removed through hydrothermal treatment without adding any reducing agent.[39] It is reported that the exfoliated GO could be reduced to graphene via hydrothermal reaction with a small amount of residual groups.[40] The SEM and TEM images of GO and GS were shown in Supporting
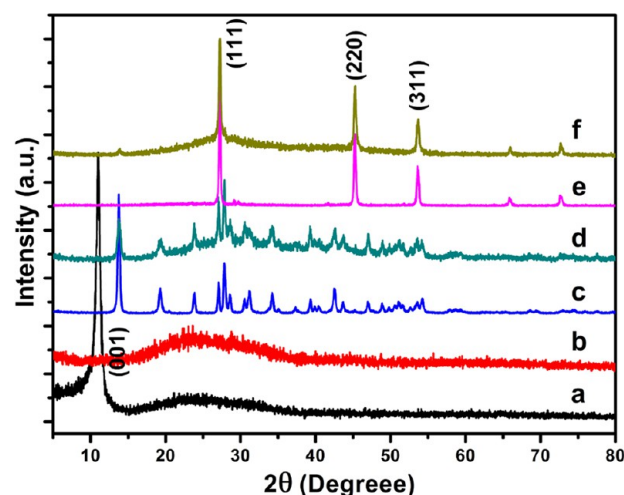

Figure 1. Typical XRD patterns of GO (a), RGO (b), ZnSe·xN_2H_4 (c), ZnSe·xN_2H_4/GS (d), ZnSe (e), and ZnSe/N-GS (f).

Information (SI) Figure S1. It is observed (SI Figure S1a and c) that GO had a crumpled layered structure with several stacking layers of the monatomic GS. After reduction by hydrothermal reaction, the reduced graphene was retained in the form of two-dimensional sheets with micrometer-long wrinkles as shown in SI Figure S1b and d. The inset pictures in SI Figure S1c and d are the selected-area electron diffraction pattern (SAED) of GO and GS, and it can be seen that the GS obtained from reduction of GO has a slightly clear six-fold pattern. It confirms that the crystal structure of the original graphite is retained in the exfoliated sheets and would improve by the hydrothermal reaction.

For ZnSe·xN_2H_4/GS (Figure 1d), the XRD pattern of the product fails to be identified among the JCPDS (Joint Committee on Powder Diffraction Standards) cards. However, it is the same as the ZnSe molecular precursors reported in ref 40, indicating that it should be an inorganic−organic hybrid semiconductor: ZnSe·xN_2H_4, which can be well repeated as Figure 1c. In additional, if EDTA−2Na was added as a chelating ligand, the products transformed to ZnSe and ZnSe/N-GS as shown in Figure 1e and f, respectively, which are in good agreement with the JCPDS card (No. 37-1463). Therefore, the EDTA-2Na can prevent the adsorption of N_2H_4 and restrict the formation of ZnSe·xN_2H_4 in the hydrothermal process. And the diffraction peak of GS also can be seen in the ZnSe/N-GS composite in Fig. 1f.

Raman spectroscopy was used for the characterization of the structure and quality of carbon materials, particularly to determine the defects, the ordered and disordered structures, and the layers of graphene.[16,41,42] Figure 2 shows the typical room-temperature Raman spectrum of ZnSe/N-GS and ZnSe·xN_2H_4/GS nanocomposites in comparison to RGO and GS. There are four typical Raman bands, which were located at around 1346, 1579, 2686, and 2935 cm^{-1}, the details were exhibited in Table 1. The band at around 1346 cm^{-1} is common for disordered sp^2 carbon and has been called the D-band and the other band at around 1579 cm^{-1} is close to that observed for well ordered graphite and is often called the G-band or E_{2g} mode, in addition, a broader 2D and 2G peaks appeared at around 2686 and 2935 cm^{-1}, which is consistent with that of the few-layer graphene. Obviously, these four bands for both ZnSe/N-GS and ZnSe·xN_2H_4/GS were down-shifted compared to GO and GS (Table 1). This should ascribe to the
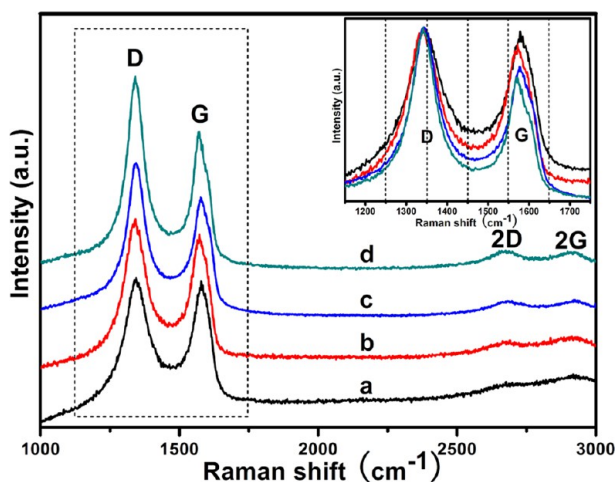
Figure 2. Raman spectra of the GO (a), GS (b), ZnSe·xN$_2$H$_4$/GS (c), and ZnSe/N-GS (d).

Table 1. D, G, 2D, 2G Band of the GO, GS, ZnSe·xN$_2$H$_4$/GS, and ZnSe/N-GS

sample	D (cm^{-1})	G (cm^{-1})	2D (cm^{-1})	2G (cm^{-1})	D/G
GO	1346	1579	2686	2935	1.04
GS	1345	1578	2684	2930	1.13
ZnSe·xN$_2$H$_4$/GS	1343	1578	2680	2921	1.28
ZnSe/N-GS	1343	1571	2677	2913	1.39

nitrogen doped into GS which is similar to the results of nitrogen-doped CNTs.[16,43] And it is also found that these four bands of the ZnSe/N-GS were down-shifted more than ZnSe·xN$_2$H$_4$/GS. This implies that nitrogen could insert into GS easily after adding EDTA−2Na, and the amount of nitrogen in ZnSe/N-GS should be more than that in ZnSe·xN$_2$H$_4$/GS composites. A further observation indicates that the ZnSe/N-GS composite shows an increased D/G intensity ratio of 1.39, compared to the other three samples of 1.28, 1.13, and 1.04. This decreasing ratio suggests the reduction of GO and much more disordered carbon structure, which also implies the nitrogen was incorporated into the graphene lattices than the ZnSe·xN$_2$H$_4$/GS composites.

For a further investigation, the XPS results were presented in Figure 3. XPS is a powerful tool to identify the chemical states in bulky material.[44−46] We can confirm the formation of nitrogen-doped graphene in both ZnSe·xN$_2$H$_4$/GS and ZnSe/N-GS composites by analysizing the binding energy (BE) values. Figure 3a and b showed the full-scale XPS spectra of ZnSe·xN$_2$H$_4$/GS and ZnSe/N-GS. The typical peaks of Se3d, C1s, N1s, O1s, and Zn2p were located at 54.9, 284.8, 401.6, 531.7, and 1022.1 eV, respectively. The high resolution C 1s spectra of ZnSe·xN$_2$H$_4$/GS and ZnSe/N-GS composites were given in Figure 3c and d. The C 1s spectra can be decomposed into three apparent spectral components at 284.8, 285.7, and 286.9 eV. The main peak at 284.8 eV corresponds to the graphite-like sp^2 C, and the small peak at 285.7 eV can be attributed to C−OH bonds or the N-sp^2 C bonds, additionally, the small peak at 286.9 eV is attributed to carbonyls (C═O).[16,44,47] The full XPS spectra and high revolution C 1s spectra were shown in SI Figure S2. In the C 1s spectrum of GO (SI Figure S2c), there are two peaks centered at about 284.7 and 287 eV, which are characteristic nose of the C−C bonded carbon atoms with sp^2 configurations and the covalent

bonds of C and O, respectively. When GO is converted to GS by the hydrothermal reaction, the peak at 287 eV disappeared, indicating the content of oxygen evidently decreases. However, the peak at 285.7 eV can not be surely identified. For a further confirmation, the high resolution N 1s spectra of ZnSe·xN$_2$H$_4$/GS and ZnSe/N-GS composites were given in Figure 3e and f. A signal deconvolution with Gaussian curve fitting points out chemically different N species in the composites, for the ZnSe/N-GS composites, the Gaussian peak at 398.8 eV can be attributed to pyrrolic-like N and oxidized nitrogen, the peak at 401.0 eV corresponds to quaternary (graphitic) N, which refers to the N atoms replacing the C atoms inside of the graphene layers, and the peak at 402.7 eV should be pyridinic-like N.[48−51] However, for the ZnSe·xN$_2$H$_4$/GS composites, a strong peak and a very weak peak were observed at 401.0 and 402.7 eV, respectively, and there was no peak at 398.8 eV. It is impossible that there would be so few pyrrolic-like N or pyridinic-like N when the N species were doped as quaternary N, obviously, the peak at 401.0 should be highly possible to ascribe as the N$_2$H$_4$ species in the ZnSe·xN$_2$H$_4$/GS composites. This means that the addition of EDTA-2Na would be helpful for the nitrogen species into graphene lattices, which is consistent with the former Raman results. Actually, EDTA as a nitrogen source can be easily inserted into the grahene lattice as reported in ref 37.

Figure 4a−d show representative SEM images of the ZnSe·xN$_2$H$_4$/GS and ZnSe/N-GS composites. It can be seen that the ZnSe·xN$_2$H$_4$/GS composites mostly were exhibited as nanosheets, as shown in Figure 4a and b, and the ZnSe/N-GS composites were exhibited as nanobelts shown in Figure 4c and d. It obviously indicates that the addition of EDTA-2Na can make the ZnSe keep the nanobelts morphology and not divide into nano sheets. The TEM images in Figure 4e and f also proved it, it can be seen that ZnSe showed a wider and longer nanobelts morphology. Additionally, the EDX spectra of GS in these two samples were obtained in Figure 4g and h. We can clearly see that the oxygen species in both samples were reduced to a very low ratio, and the nitrogen species in ZnSe/N-GS was higher than in ZnSe·xN$_2$H$_4$/GS composites. This result demonstrates that the addition of EDTA-2Na would benefit for the doping of nitrogen, and make the nitrogen ratio in the GS of ZnSe/N-GS higher than that in ZnSe·xN$_2$H$_4$/GS composites. This is consistent with the former results. The high revolution TEM images of GS in both samples were presented in SI Figure S3, the atomic arrangement of both samples (as shown in SI Figure S3c and d, respectively) can be seen from the magnified HRTEM images (white dish region in SI Figure S3a and b), in which GS in ZnSe·xN$_2$H$_4$/GS composites showed a more regular six-member ring except few irregular atoms, and for GS in ZnSe/N-GS composites, most of the atoms is irregular and only few regular six-member rings. This also implies that there should be more nitrogen get into the graphene lattices and make the atomic arrangement disorder when adding with EDTA−2Na. Additionally, the EDX spectra of ZnSe·xN$_2$H$_4$ and ZnSe are shown in SI Figure S4. In addition to the Zn and Se peaks, it clearly indicats that the nitrogen species in ZnSe·xN$_2$H$_4$ were larger than that in ZnSe. Thus, the whole hydrothermal process can be illustrated by Scheme 1, when EDTA−2Na was added into the mixed solution, the ZnSe·xN$_2$H$_4$ would transform to ZnSe and the nitrogen species would be more easily inserted into the graphene lattices. It was reported that nitrogen-doping could convert graphene into an n-type semiconductor.[15,16,37] Therefore, the presented ZnSe/N-GS would show an enhanced
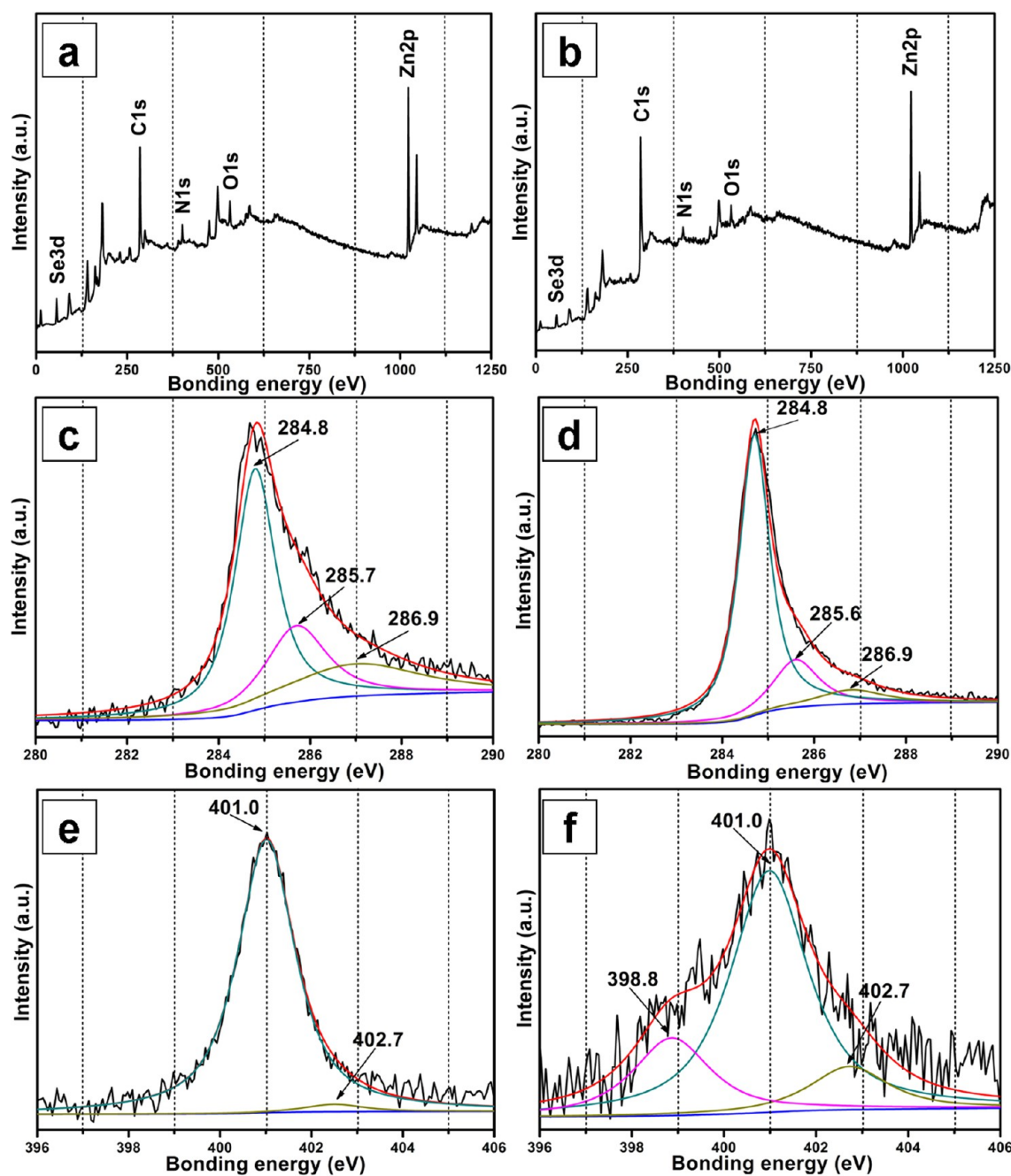
Figure 3. Full XPS spectra of ZnSe·xN$_2$H$_4$/GS (a) and ZnSe/N-GS (b), high-resolution XPS spectra of C 1s for ZnSe·xN$_2$H$_4$/GS (c) and ZnSe/N-GS (d), and N1s for ZnSe·xN$_2$H$_4$/GS (e) and ZnSe/N-GS (f).

electrical and other properties compared to ZnSe·xN$_2$H$_4$/GS composites. For a deep investigation, the CL spectra were obtained below.

As shown in Figure 5a, the peak of the pure ZnSe is located at 442.5 eV, which is corresponding to the bandgap of ZnSe (2.67).[24] However, compared to the pure ZnSe, the CL intensity of ZnSe·xN$_2$H$_4$ and ZnSe/N-GS composites showed a decreasing tendency, and the ZnSe·xN$_2$H$_4$ composites showed a very huge decrease. According to the literature,[52−54] the work function of graphene and the conduction band of bulk ZnSe is −4.6 and −4.84 eV, respectively, and it is also well known that the beam energy is much higher than the bandgap of ZnSe. Then, for the ZnSe·xN$_2$H$_4$ composites, the electrons in the valence band would excited much higher than the conduction

band, due to the slightly higher energy level of GS and its excellent electrical conductivity properties, the excited electrons would transfer to GS and hard to injected to the conduction band of ZnSe as part a showed in Fig. 5b, consequently, the CL intensity would largely decreased. This consisted with many reported results that the graphene would act as electron separator in many graphene based materials.[28−33] But there would be some difference for the ZnSe/N-GS composites, compared with the relatively large work function of pure graphene, N-doped reduced graphene revealed significantly lowered work function.[52] Then, ZnSe and the nitrogen doped GS would act as heterosystems and create p−n junctions. As a result, the electrons trapped by the nitrogen doped GS would transfer from its conduction band to the conduction band of
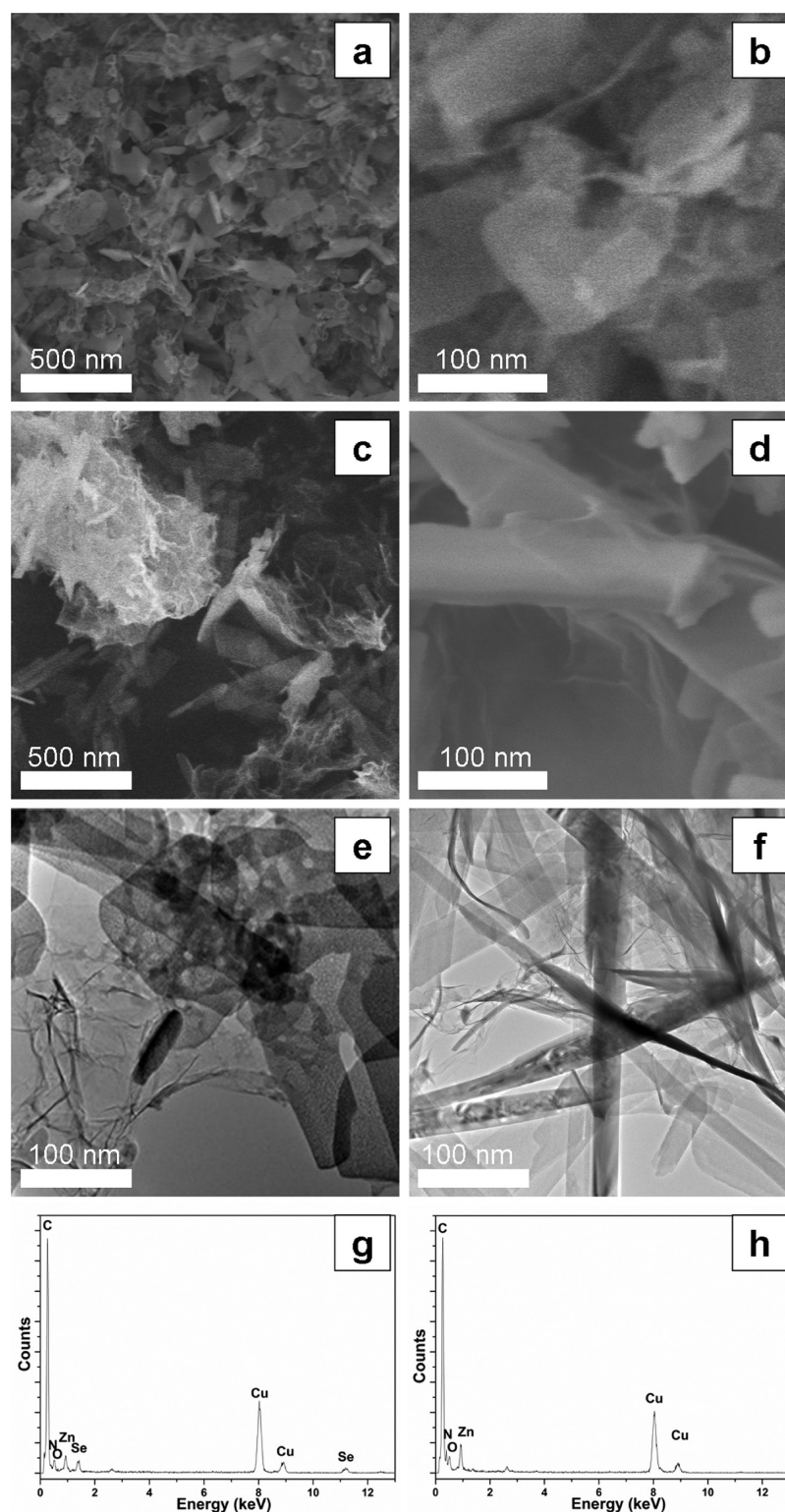
8417

dx.doi.org/10.1021/am401701y | ACS Appl. Mater. Interfaces 2013, 5, 8414−8422

Figure 4. Low (a) and high resolution (b) SEM images of ZnSe·xN$_2$H$_4$/GS, low (c) and high (d) SEM images of ZnSe/N-GS, TEM images of ZnSe·xN$_2$H$_4$/GS (e) and ZnSe/N-GS (f), and EDX spectra of GS in ZnSe·xN$_2$H$_4$/GS (g) and ZnSe/N-GS (h).

ZnSe as part b showed in Figure 5b, obviously, the CL intensity would be higher than the one of ZnSe·xN$_2$H$_4$ composites. Additionally, there is also a slightly shift from 442.5 to 467.6 and 474.7 eV, respectively. This should be due to the Schottky barrier between GS and ZnSe/ZnSe·xN$_2$H$_4$, the energy barrier would make the conduction and valence band of ZnSe/ZnSe·xN$_2$H$_4$ at the junction area bend to a higher energy level, then

make the band gap showed a slightly decrease and the CL spetra would shift to a lower energy. This implies these GS based composites have a potential applicability in photocatalysis.

On the basis of the above results, we also tested the photocatalytic activity of these ZnSe based samples for the photodegradation of methylene blue (MB) under visible light
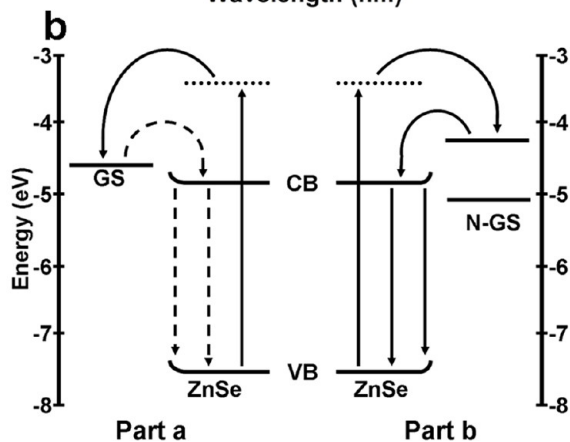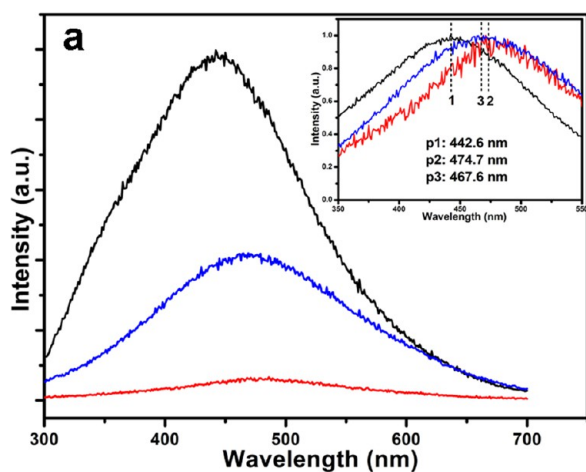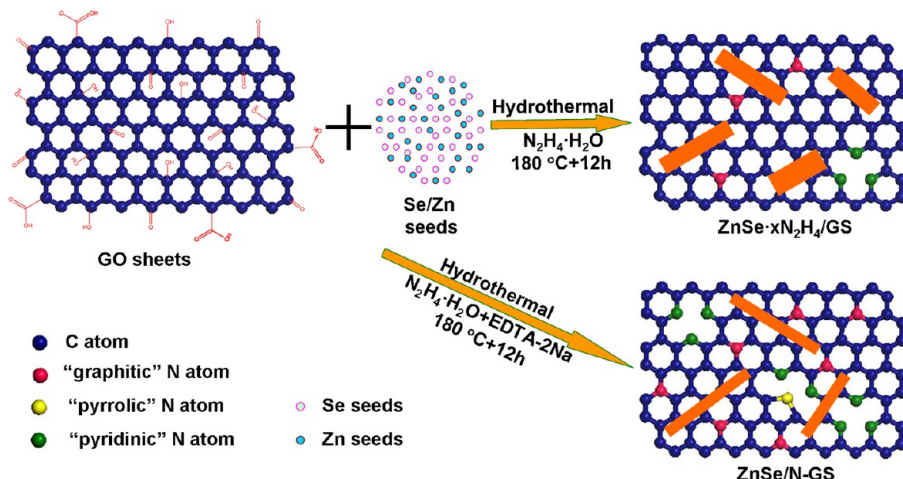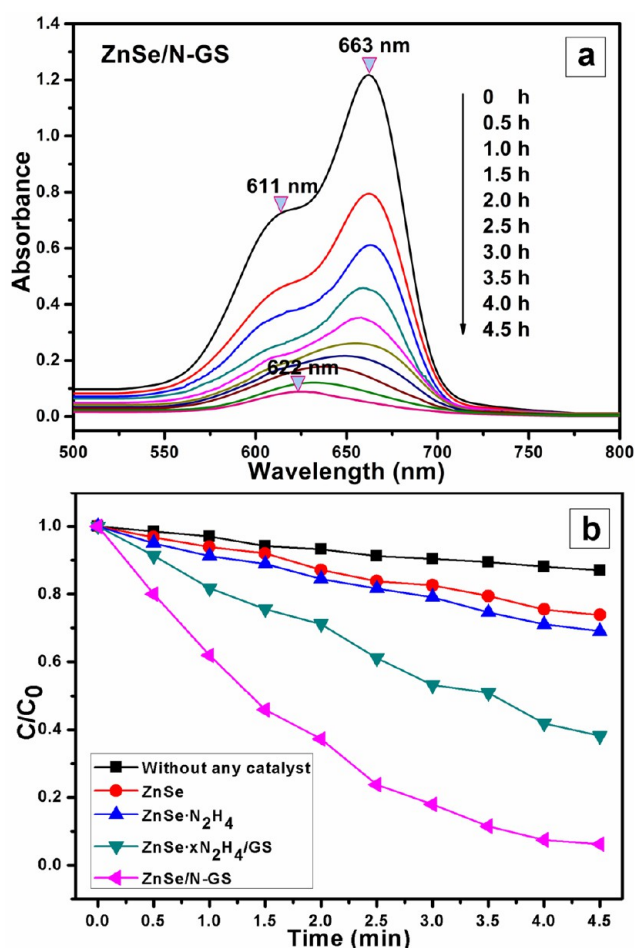
Scheme 1. Flow Chart for Preparation of ZnSe·xN$_2$H$_4$/GS and ZnSe/N-GS Composites by a Hydrothermal Treatment

Figure 5. CL spectra of different samples (a) and scheme of the electroluminescence process (b).

Figure 6. Time profile of MB absorbance spectra observed during incubation with ZnSe/N-GS under visible light irradiation (a) and photodegradation of methylene blue (MB) under visible light ($\lambda > 420$ nm) by different samples (b).

range. Figure 6a shows time profile of MB absorbance spectra observed during the incubation with ZnSe/N-GS composites under visible light irradiation. The absorption peaks at 611 and 663 nm in Figure 6a correspond to dimers and monomers of MB, respectively.[56] Another peak at 622 nm corresponds to the formation of the demethylated MB during oxidative decomposition.[57] For the evaluation of degradation kinetics of MB, we measured the change of main absorption peak of MB at 663 nm as shown in Figure 6b, which had been widely used according to other work.[56,58−60] While MB was slightly degraded without

adding any catalysts, both of ZnSe·xN$_2$H$_4$ and ZnSe showed a slightly enhanced photocatalysis properties (remain 69.0% and 73.8%, respectively). However, for the GS-based ZnSe·xN$_2$H$_4$/GS and ZnSe/N-GS composites, it shows significantly enhanced photocatalytic performance, especially for the ZnSe/N-GS composites. It still remain 38.2% for ZnSe·

xN$_2$H$_4$/GS composites after 4.5 h, while it is less than 10% for the ZnSe/N-GS.

On the one hand, as the ZnSe·xN$_2$H$_4$ and ZnSe were dispersed on the surface of the GS/N-GS sheets, the adsorption of MB on the catalysts could be attributed to two parts, the adsorption of MB on the surface of the GS/N-GS and the surface of the ZnSe·xN$_2$H$_4$/ZnSe. The former seems to be much more favorable because of its giant p-conjugational plane, which strongly interacts with MB molecules via a $\pi-\pi$ stacking with a face-to-face orientation.[34,61] And actually, the pure ZnSe·xN$_2$H$_4$/ZnSe only showed a less adsorption properties as shown in Table 2. It was obvious that, after equilibrium in the

Table 2. Remaining Concentration Fraction of Dyes after Dark Adsorption

stirring time (min)		0 (initial)	30	60	120
remained concentration	ZnSe	100	89	84	83
	ZnSe·xN$_2$H$_4$	100	88	83	83
	ZnSe·xN$_2$H$_4$/GS	100	82	79	78
	ZnSe/N-GS	100	83	80	79

dark for 30 min, the MB molecules remained 89%, 88%, 82%, and 83%, respectively, and after 120 mins dark adsorption process, the dye molecules remained 83%, 83%, 78%, and 79%, which still showed slightly enhanced adsorption abilities for the GS/N-GS based composites. On the other hand, as discussed in the CL spectra, it implied that composite with GS and nitrogen doped GS would make the electron transfer different to the pure ZnSe. Thus, we can attribute the significantly enhanced photocatalytic performance of ZnSe·xN$_2$H$_4$/GS and ZnSe/N-GS composites under visible light to the changed electron transformation.

An excited dye can transfer electrons to the conduction band of ZnSe or other semiconductors to generate reactive oxygen species (ROSs) as shown in Scheme 2a. The dye being both a sensitizer and a pollutant is decomposed.[62−64] According to the literature,[52,55,65] the work function of excited MB, graphene, and the conduction band of pure ZnSe are −3.60, −4.60, and −4.84 eV, respectively, and the nitrogen-doped GS would show a lower work function than GS. Considering the potential of the conduction band (−4.84 eV) and valence band (−7.5 eV) of ZnSe, direct electron transfer from MB* to graphene is not only thermodynamically favorable, but also much more feasible than ZnSe (Scheme 2b and c). To prove this, the fluorescence lifetimes of MB were determined in different suspensions as shown in Figure 7. MB solution has a strong fluorescence with a lifetime of about 1.638 ns (as shown in Figure 7) because of its conjugated xanthene structure. Upon addition of pure ZnSe, MB could be adsorbed on the ZnSe surface, the fluorescence lifetime of MB decreased to 1.213 ns (as shown in Figure 7) because of the electron transfer from MB* to ZnSe. As GS was introduced into the MB solution, the related lifetime was remarkably reduced to 0.014 ns, indicating a strong electron transfer between MB* and GS. The related lifetime after adding of N-GS showed a slightly increase to 0.208 ns, this should be due to its disordered carbon structure with the nitrogen dope. Then, the significantly enhanced photocatalytic performance of ZnSe·xN$_2$H$_4$/GS and ZnSe/N-GS samples in our work can be well understood. Furthermore, according to the discussion above, the interaction mode of MB with GS/N-GS could be very different to the anchored on the ZnSe surface via the ethyl

Scheme 2. Suggested Mechanism for the Photocatalytic Degradation of MB by Pure ZnSe (a), ZnSe·xN$_2$H$_4$/GS (b), and ZnSe/N-GS (c)
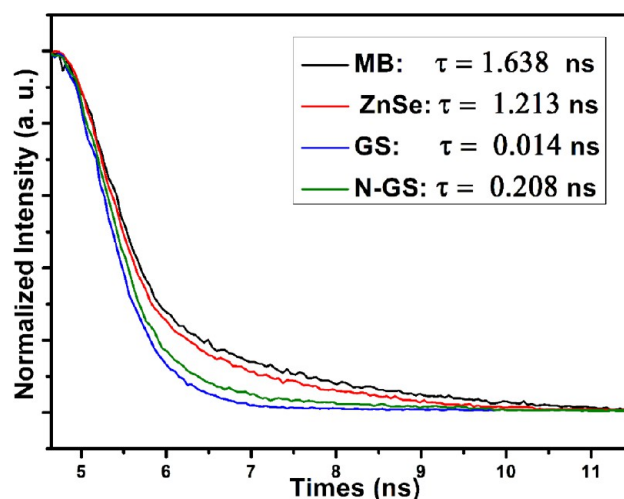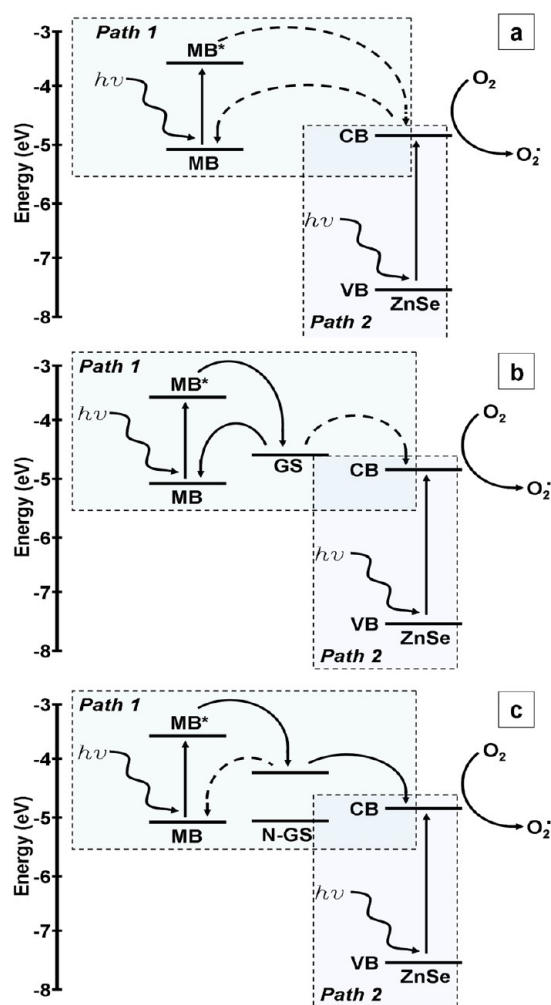

Figure 7. Lifetime of MB solution with adding different samples.

groups or the carboxyl groups. It is possible due to its giant p-conjugational plane, which would strongly adsorb on the surface of GS/N-GS via a $\pi-\pi$ stacking with a face-to-face orientation.[34,61] Thus, if the injected electrons were not duly transferred, they were easily recombined with surface adsorbed

8420

dx.doi.org/10.1021/am401701y | ACS Appl. Mater. Interfaces 2013, 5, 8414−8422

MB*[+] radicals (Scheme 2b), which would lower the degradation efficiency as shown in some other organic pollution degradation.[66] For the ZnSe·xN$_2$H$_4$/GS composites, this recombination is unavoidable as Scheme 2b showes, and its photocatalytic properties would be affected. Because plenty of nitrogen species get into the graphene lattices, it would convert nitrogen doped graphene into an n-type semiconductor,[52,55,65] and this would significantly reduce the work function than pure graphene;[52] thus, the ZnSe/N-GS composites would act as heterosystems and create p−n junctions. The potential differences between N-GS and the conduction band of ZnSe would became larger, this would force the injected electrons on N-GS move to conduction band of ZnSe more easily which spatially separated MB* and electrons and retarding the recombination process; Furthermore, the resulted graphene lattice is a disordered carbon structure, then the injected electrons on N-GS move to MB*[+] radicals would slightly be rusticated, and this decreases the recombination process as shown in Scheme 2c. Thus, the significant enhanced photo-catalytic properties can be achieved.

CONCLUSIONS

In summary, both ZnSe·xN$_2$H$_4$/GS and ZnSe/N-GS composites have been successfully and directly produced via a facile, catalyst-free one-pot hydrothermal method at a low temperature, in which Zn(Ac)$_2$·2H$_2$O and Na$_2$SeO$_3$·5H$_2$O powders as the reactants, N$_2$H$_4$·H$_2$O and EDTA−2Na as the reductant and the nitrogen source. It was found that adding of EDTA−2Na would make the ZnSe·xN$_2$H$_4$ converted to ZnSe and more nitrogen species can be inserted into the graphene lattice. Due to the strongly interacts between GS and MB molecules via a π−π stacking with a face-to-face orientation, the direct electron transfer from MB* to graphene is not only thermodynamically favorable, but also much more feasible than ZnSe. This would result in an enhanced photocatalytic performance for the ZnSe·xN$_2$H$_4$/GS and ZnSe/N-GS composite in comparison to ZnSe and ZnSe·xN$_2$H$_4$. Additionally, the nitrogen-doping can convert graphene into an n-type semiconductor making the electron transfer from N-GS to the conduction band of ZnSe more easily, and this results in a better photocatalytic performance for ZnSe/N-GS composite in comparison to ZnSe·xN$_2$H$_4$/GS composites. These results indicate that both ZnSe·xN$_2$H$_4$/GS and ZnSe/N-GS composite could be used as selective photocatalysts for the degradation of contaminant molecules which have potential application in wastewater treatment. Because graphene exhibits excellent physical and chemical properties, it is necessary to synthesize other new composites based on graphene sheets. Our simple method could be readily extended to prepare other new graphene/semiconductor nanocomposites, which could be promising for various applications, such as in lithium ion batteries, the environmental protection issues and fuel cells, and nanodevices.

ASSOCIATED CONTENT

ⓈSupporting Information

Preparation of monolayer GO dispersion and catalyst activity experimental, SEM, HRTEM micrographs, XPS, and EDX spectra of GO/GS. This material is available free of charge via the Internet at http://pubs.acs.org.

AUTHOR INFORMATION

Corresponding Authors
*Bitao Liu: e-mail liubitao007@163.com.
*Liangliang Tian: e-mail tianll07@163.com.

Notes
The authors declare no competing financial interest.

ACKNOWLEDGMENTS

REFERENCES

(1) Geim, A. K.; Novoselov, K. S. Nat. Mater. 2007, 6, 183−191.
(2) Morozov, S. V.; Novoselov, K. S.; Katsnelson, M. I.; Schedin, F.; Ponomarenko, L. A.; Jiang, D.; Geim, A. K. Phys. Rev. Lett,. 2006, 97, 016801−016804.
(3) Balandin, A. A.; Ghosh, S.; Bao, W. Z.; Calizo, I.; Teweldebrhan, D.; Miao, F.; Lau, C. N. Nano Lett. 2008, 8, 902−907.
(4) Chen, J. H.; Jang, C.; Xiao, S. D.; Ishigami, M.; Fuhrer, M. S. Nat. Nanotechnol. 2008, 3, 206−209.
(5) Lee, C. G.; Wei, X.; Kysar, J. W.; Hone, J. Science 2008, 321, 385−388.
(6) Stoller, M. D.; Park, S. J.; Zhu, Y. W.; An, J. H.; Ruoff, R. S. Nano Lett. 2008, 8, 3498−3502.
(7) Sun, Y. Q.; Wu, Q.; Shi, G. Q. Energy Environ. Sci. 2011, 4, 1113−1132.
(8) Nair, R. R.; Blake, P.; Grigorenko, A. N.; Novoselov, K. S.; Booth, T. J.; Stauber, T.; Peres, N. M. R.; Geim, A. K. Science 2008, 20, 1308.
(9) Park, S.; Ruoff, R. S. Nat. Nanotechnol. 2009, 4, 217−224.
(10) Dmitry, V. K.; Amanda, L. H.; Alexander, S.; Jay, R. L.; Ayrat, D.; Price, B. K.; James, M. T. Nature 2009, 458, 872−876.
(11) Luo, B.; Liu, S. M.; Zhi, L. J. Small 2011, 8, 630−646.
(12) Sutter, P. W.; Flege, J. I.; Utter, E. A. Nat. Mater. 2008, 7, 406−411.
(13) Reina, A.; Jia, X. T.; Ho, J.; Nezich, D.; Son, H. B.; Bulovic, V.; Mildred, S.; Dresselhaus, M. S.; Kong, J. Nano Lett. 2009, 9, 30−35.
(14) Zhi, L. J.; Müllen, K. J. Mater. Chem. 2008, 18, 1472−1484.
(15) Li, X.; Wang, H.; Robinson, J. T.; Sanchez, H.; Diankov, G.; Dai, H. J. Am. Chem. Soc. 2009, 131, 15939−15944.
(16) Sheng, Z. H.; Shao, L.; Chen, J. J.; Bao, W. J.; Wang, F. B.; Xia, X. H. ACS Nano 2011, 5, 4350−4358.
(17) Luo, Z. Q.; Lim, S. h.; Tian, Z. Q.; Shang, J. Z.; Lai, L. F.; Donald, B. M.; Fu, C.; Shen, Z. X.; Yu, T.; Lin, J. Y. J. Mater. Chem. 2011, 21, 8038−8044.
(18) Panchakarla, L. S.; Subrahmanyam, K. S.; Saha, S. K.; Govindaraj, A.; Krishnamurthy, H. R.; Waghmare, U. V.; Rao, C. N. R. Adv. Mater. 2009, 21, 4726−4730.
(19) Cabria, I.; López, M. J.; Alonso, J. A. J. Chem. Phys. 2005, 123, 204721−1204729.
(20) Dong, X. C.; Fu, D. L.; Fang, W. J.; Shi, Y. M.; Chen, P.; Li, J. Small 2009, 5, 1422−1426.
(21) Jeong, H. M.; Lee, J. W.; Shin, W. H.; Choi, Y. J.; Shin, H. J.; Kang, J. K.; Choi, J. W. Nano Lett. 2011, 11, 2472−2477.
(22) Alivisatos, A. P. Science 1996, 271, 933−937.
(23) Nirmal, M.; Brus, L. Acc. Chem. Res. 1999, 32, 407−414.
(24) Hines, M. A.; Sionnest, P. G. J. Phys. Chem. B 1998, 102, 3655−3657.
(25) Peng, Q.; Dong, Y. J.; Li, Y. D. Angew. Chem., Int. Ed. 2003, 42, 3027−3030.
(26) Zhang, L. H.; Yang, H. Q.; Yu, J.; Shao, F. H.; Li, L.; Zhang, F. H.; Zhao, H. J. Phys. Chem. C 2009, 113, 5434−5443.
(27) Yao, W. T.; Yu, S. H.; Huang, X. Y.; Jiang, J.; Zhao, L. Q.; Pan, L.; Li, J. Adv. Mater. 2005, 17, 2799−2802.
(28) Zheng, J. B.; He, Y. P.; Sheng, Q. L.; Zhang, H. F. J. Mater. Chem. 2011, 21, 12873−12879.
(29) Xin, Y. C.; Liu, J. G.; Zhou, Y.; Liu, W. M.; Gao, J. A.; Xie, Y.; Yin, Y.; Zou, Z. G. J. Power Sources 2011, 196, 1012−1018.

8421

dx.doi.org/10.1021/am401701y | ACS Appl. Mater. Interfaces 2013, 5, 8414−8422

(30) Chen, S.; Zhu, J. W.; Wu, X. D.; Han, Q. F.; Wang, X. *ACS Nano* 2010, *4*, 2822−2830.

(31) Liu, B.; Huang, Y.; Wen, Y.; Du, L.; Zeng, W.; Shi, Y.; Zhang, F.; Zhu, G.; Xu, X.; Wang, Y. *J. Mater. Chem.* 2012, *22*, 7484−7491.

(32) Wang, Y.; Guo, C. X.; Liu, J. H.; Chen, T.; Yang, H. B.; Li, C. M. *Dalton Trans.* 2011, *40*, 6388−6391.

(33) Li, B. J.; Cao, H. Q. *J. Mater. Chem.* 2011, *21*, 3346−3349.

(34) Zhang, H.; Lv, X. J.; Li, Y. M.; Wang, Y.; Li, J. H. *ACS Nano* 2010, *4*, 380−386.

(35) Wang, P.; Jiang, T. F.; Zhu, C. Z.; Zhai, Y. M.; Wang, D. J.; Dong, S. J. *Nano. Res* 2010, *3*, 794−799.

(36) Liang, Y. Y.; Li, Y. G.; Wang, H. L.; Zhou, J. G.; Wang, J.; Regier, T.; Dai, H. J. *Nat. Mater.* 2011, *10*, 780−786.

(37) Chen, P.; Xiao, T. Y.; Li, H. H.; Yang, J. J.; Wang, Z.; Yao, H. B.; Yu, S. H. *ACS Nano* 2012, *6*, 712−719.

(38) Xu, Y. X.; Bai, H.; Lu, G. W.; Li, C.; Shi, G. G. *J. Am. Chem. Soc.* 2008, *130*, 5856−5857.

(39) Jeong, H. K.; Lee, Y. P.; Lahaye, R. J. W. E.; Park, M. H.; An, K. H.; Kim, I. J.; Yang, C. W.; Park, C. Y.; Ruoff, R. S.; Lee, Y. H. *J. Am. Chem. Soc.* 2008, *130*, 1362−1366.

(40) Ni, Y. H.; Zhang, L.; Zhang, L.; Wei, X. W. *Cryst. Res. Technol.* 2008, *43*, 1030−1035.

(41) Das, A.; Pisana, S.; Chakraborty, B.; Piscanec, S.; Saha, S. K.; Wangmare, U. V.; Novoselov, K. S.; Krishnamurthy, H. R.; Geim, A. K.; Ferrari, A. C.; Sood, A. K. *Nat. Nanotechnol.* 2008, *3*, 210−215.

(42) Dresselhaus, M. S.; Jorio, A.; Hofmann, M.; Dresselhaus, G.; Saito, R. *Nano Lett.* 2010, *10*, 751−758.

(43) Panchakarla, L. S.; Govindaraj, A.; Rao, C. N. R. *ACS Nano* 2007, *1*, 494−500.

(44) Wang, Y.; Shao, Y. Y.; Matson, D. W.; Li, J. H.; Lin, Y. H. *ACS Nano* 2010, *4*, 1790−1798.

(45) Park, S. J.; Hu, Y. C.; Hwang, J. O.; Lee, E. S.; Casabianca, L. B.; Cai, W. W.; Potts, J. R.; Ha, H. W.; Chen, S. S.; Oh, J. H.; Kim, S. O.; Kim, Y. H.; Ishii, Y.; Ruoff, R. S. *Nat. Commun.* 2012, *1643*, 1−8.

(46) Stankovich, S.; Dikin, D. A.; Piner, R. D.; Kohlhaas, K. A.; Kleinhammes, A.; Jia, Y. Y.; Wu, Y.; Nguyen, S. B. T.; Ruoff, R. S. *Carbon* 2007, *45*, 1558−1565.

(47) Wei, D. C.; Liu, Y. Q.; Wang, Y.; Zhang, H. L.; Huang, L. P.; Yu, G. *Nano Lett.* 2009, *9*, 1752−1758.

(48) Xu, F.; Minniti, M.; Barone, P.; Sindona, A.; Bonanno, A.; Oliva, A. *Carbon* 2008, *46*, 1489−1496.

(49) Wang, X, B.; Liu, Y. Q.; Zhu, D. B.; Zhang, L.; Ma, H. Z.; Yao, N.; Zhang, B. L. *J. Phys. Chem. B* 2002, *106*, 2186−2190.

(50) Long, D. H.; Li, W.; Ling, L. C.; Miyawaki, J.; Mochida, I.; Yoon, S. H. *Langmuir* 2010, *26*, 16096−16102.

(51) Brisson, P. Y.; Darmstadt, H.; Fafard, M.; Adnot, A.; Servant, G.; Soucy, G. *Carbon* 2006, *44*, 1438−1447.

(52) Hwang, J. O.; Park, J. S.; Choi, D. S.; Kim, J. Y.; Lee, S. H.; Lee, K. E.; Kim, Y. H.; Song, M. H.; Yoo, S.; Kim, S. O. *ACS Nano* 2012, *6*, 159−167.

(53) Yu, Y. J.; Zhao, Y.; Ryu, S.; Brus, L. E.; Kim, K. S.; Kim, P. *Nano Lett.* 2009, *9*, 3430−3434.

(54) Hibini, H.; Kageshima, H.; Kotsugi, M.; Maeda, F.; Guo, F. Z.; Watanabe, Y. *Phys. Rev. B* 2009, *79*, 125437−125443.

(55) Swank, W. E.; Comber, P. G. L. *Phys. Rev.* 1967, *153*, 844−849.

(56) An, C.; Peng, S.; Sun, Y. *Adv. Mater.* 2010, *22*, 2570−2574.

(57) Zhang, T.; Oyama, T.; Aoshima, A.; Hidaka, H.; Zhao, J.; Serpone, N. *J. Photochem. Photobiol. A* 2001, *140*, 163−172.

(58) Soni, S. S.; Henderson, M. J.; Bardeau, J. F.; Gibaud, A. *Adv. Mater.* 2008, *20*, 1493−1498.

(59) Elmalem, E.; Sauders, A. E.; Costi, R.; Salant, A.; Banin, U. *Adv. Mater.* 2008, *20*, 4312−4318.

(60) Qiu, X.; Zhao, Y.; Burda, C. *Adv. Mater.* 2007, *19*, 3995−3999.

(61) Ng, Y. H.; Lightcap, I. V.; Goodwin, K.; Matsumure, M.; Kamat, P. V. *J. Phys. Chem. Lett.* 2010, *1*, 2222−2227.

(62) Chatterjee, D.; Dasgupta, S. *J. Photochem. Photobiol, C* 2005, *6*, 186−205.

(63) Zhao, D.; Chen, C.; Wang, Y.; Ma, W.; Zhao, J.; Rajh, T.; Zang, L. *Environ. Sci. Technol.* 2008, *42*, 308−314.

(64) Ji, P. F.; Zhang, J. L.; Chen, F.; Anpo, M. *Appl. Catal., B* 2009, *85*, 148−154.

(65) Ocak, Y. S.; Kulakci, M.; Kilicoglu, T.; Turan, R.; Akkilic, K. *Synth. Met.* 2009, *159*, 1603−1607.

(66) Kamat, P. V. *Chem. Rev.* 1993, *93*, 267−300.